AIP | Journal of Applied Physics

Low-frequency Raman scattering from Si/Ge nanocrystals in different matrixes caused by acoustic phonon quantization

Venu Mankad, Sanjeev K. Gupta, Prafulla K. Jha, N. N. Ovsyuk, and G. A. Kachurin

Citation: J. Appl. Phys. **112**, 054318 (2012); doi: 10.1063/1.4747933
View online: http://dx.doi.org/10.1063/1.4747933
View Table of Contents: http://jap.aip.org/resource/1/JAPIAU/v112/i5
Published by the American Institute of Physics.

Low-frequency Raman scattering from Si/Ge nanocrystals in different matrixes caused by acoustic phonon quantization

Venu Mankad,[1] Sanjeev K. Gupta,[1] Prafulla K. Jha,[1,a)] N. N. Ovsyuk,[2] and G. A. Kachurin[3]
[1]*Department of Physics, Maharaja Krishnakumarsinhji Bhavnagar University, Bhavnagar 364 001, India*
[2]*Institute for Geology and Mineralogy, Siberian Branch, Russian Academy of Sciences, Novosibirsk 630090, Russia*
[3]*Institute of Semiconductor Physics, Novosibirsk 630090, Russia*

(Received 16 November 2011; accepted 20 July 2012; published online 10 September 2012; corrected 12 September 2012)

Si and Ge nanocrystals (nc-Si and nc-Ge) with average sizes in the range of 6 and 6.3 nm, embedded in SiO_2/GeO_2 matrix, were fabricated and their acoustic-phonon vibrational properties were investigated using two different approaches by considering the elastic continuum model and fixed boundary condition. The breathing and quadrupolar modes are found in the spectra. The presence of medium significantly affects the phonon peaks and results into the broadening of the modes which is more in the case of elastically similar materials. The phonon line width is found to depend inversely on the size, similar to that reported experimentally. Using first and second-order optical modes, the electron-phonon coupling strengths have been estimated. The result shows that e-p coupling strength is more in the case of elastically dissimilar materials. © *2012 American Institute of Physics*. [http://dx.doi.org/10.1063/1.4747933]

I. INTRODUCTION

Nanocrystalline (nc-) Si and Ge are of considerable current interest because of its potential applications in future high-speed micro-electronics and memory devices. When the size of Si reduces in the scale to few nm, its opto-electronic properties change dramatically over its bulk value. Apart from the well known size-induced quantum confinement in nc-Si, there exist several studies on the vibrational properties of nc-Si.[1–4] Ge nanocrystals (NCs) based memory devices have shown great potentials for future memory devices since they exhibit high-speed programming and low-voltage operation as compared with Si NCs based devices.[5] There are many techniques to synthesize Si and Ge-NC's (Refs. 6–8), but ion implantation and subsequent thermal annealing method has been established as an efficient way to form embedded NCs in solids.[9,10] In contrast to nc-Si, nc-Ge shows stronger confinement effect resulting in a direct band gap semiconductor nature.[11,12] However, studies have shown that the optical properties of the nc-Ge are dominated by the defects[13] and hence its properties are different than its bulk counterpart. Low-frequency Raman scattering (LFRS) from nanocrystals is an interesting subject of current experimental and theoretical investigations in the field of nanoscience and nanotechnology.[14–24] Experimental determination of the low-frequency modes is often difficult since the scattering cross-section is quite low for small sized NCs, whereas for the larger size NCs, low-frequency modes fall in a region where the Rayleigh tail dominates the scattering intensity. In contrast to the case of Si NCs embedded in SiO_2, Ge NCs embedded in SiO_2 have sharp change in acoustic impedance, since there is large difference in densities as Ge is much heavier than SiO_2.[25] Therefore, the Ge NCs may co-exist with the interfacial binary Ge-Si component in which the Ge-Si bonds modify the surface vibrational properties of the Ge NCs and make the surface modes sensitive to the interfacial Si content. Furthermore, it is noted that Ge and Si NC's are surrounded by SiO_2/GeO_2 that impedes the vibration of Ge/Si atoms at the surface of the NC.

Raman scattering probes the vibrational states of the particles such as the confined acoustic, optical phonons, and surface phonon modes. It also provides an understanding of electron-phonon (e-p) interactions. This has led to several investigations of acoustic vibrations of spherical nanoparticles, particularly the semiconductor nanoparticles leading to an understanding of the role of vibrations in the performance of some optical devices (for example, in electronic dephasing due to emission of phonons).[5,6] The low frequency phonon modes (acoustic vibrations) of the elastic sphere (nanoparticles) having frequency very low compared to laser light lead to variations in the dielectric response of the sphere to the light and bear a unique signature of their structural and mechanical properties.

To explain the low-frequency acoustic modes in free and embedded NCs systems, Lamb's theory[26] has been extensively used in recent past.[14–19] The low-frequency Raman scattering has widely been used to study the size effect of surface acoustic-phonon vibration frequency in nanoparticles such as SnO_2,[27] Ag in silica,[28] CeO_2 in SiO_2 (Ref. 29), $CdTe_{1-x}Se_x$ and CdS_xSe_{1-x} in glass,[30] and Si cluster in porous Si.[31,32] An inverse relationship between the vibrational frequency and particle diameter was often reported, as predicted by Lamb's theory[26] for the vibration of a homogenous elastic sphere with free boundary condition. Two sets of vibrational modes corresponding to spheriodal and torsional vibrational modes have been derived for spherical particles. Group theory predicts that the spherical modes are observed in Raman scattering where as torsional modes are not observed.[22,33] While, Wu *et al.*[34] observed the

a)Electronic mail: prafullaj@yahoo.com.

torsional modes ($l=1$, $n=0$ and $l=2$, $n=0$) in nanocrystalline silicon which they attributed to the nonspherical shape of the particle, Ovsyuk and Novikov[35] observed the torsional mode ($l=1$, $n=0$) in nanocrystal CdS in GeO_2 matrix with a frequency ratio of ~0.72 and attributed to the particle-matrix interaction similar to the recent argument of Ivanda *et al.*[36] In recent studies on $CdS_{1-x}Se_x$ embedded in glass, we also observed the torsional modes.[30]

In this paper, we present a systematic study of the low-frequency Raman scattering from Si and Ge nanocrystals (nc-Si and nc-Ge) with the particle size of 6 and 6.3 nm, embedded in SiO_2/GeO_2 matrix. The preparation of Si and Ge nanocrystals and their characterization with some preliminary results on low-frequency phonon modes are discussed elsewhere.[37] For this, we have considered three sets of samples having two different sizes. In order to identify the peaks appearing in the measured Raman spectra, the calculation of the low frequency phonon modes of Si and Ge nanocrystals embedded in SiO_2/GeO_2 matrix has been performed using core-shell model (CSM) (Refs. 20, 28–30, and 36) as well as classical Lamb's model.[26] The CSM, which is an extension of Lamb's model,[30,37] considers the presence of medium and estimates the vibrational modes resulting from the nanoparticle-medium interaction. The possible reasons for the appearance of modes in the Raman spectra are discussed. We have also discussed phonon linewidth, optical Raman spectra (Si/SiO_2, Ge/SiO_2, and Ge/GeO_2) and electron-phonon (e-p) interaction from Raman intensity. However, to our knowledge, there are no studies in the literature where electron-phonon coupling strength has been measured for such systems. The rest of the paper is organized as follows; a brief details of theoretical consideration performed are presented in Sec. II. We present the results and discussion in Sec. III. Then paper concludes with a summary in Sec. IV.

II. THEORETICAL CONSIDERATIONS

Confined acoustic phonons in nanoparticles give rise to low-frequency modes in the vibrational spectra of the materials. These low-frequency phonon modes of Si and Ge nanocrystals (nc-Si and nc-Ge) with average sizes in the range of 6 and 6.3 nm, embedded in SiO_2/GeO_2 matrix can be obtained by solving the equation of motion of a homogeneous, free standing elastic sphere, first proposed by Lamb[26] and later used by others.[19,30,36–43]

In order to understand the key features of the experimental Raman spectra, the vibrations of the Si and Ge nanocrystals (nc-Si and nc-Ge) are calculated using two approaches: (i) using the original Lamb's approach[26] and (ii) CSM applicable to both free as well embedded nanoparticles.[37–45] However, the present equation for the homogenous, isotropic medium is written as[26]

$$(\lambda+2\mu)\,\vec{\nabla}(\vec{\nabla}.\vec{u}) - \mu\vec{\nabla}\times(\vec{\nabla}\times\vec{u}) = \rho\ddot{\vec{u}}, \qquad (1)$$

where λ and μ are Lame's constants and ρ is the mass density of nanoparticle, which are related to each other by the expressions $V_l=\sqrt{\frac{2\mu+\lambda}{\rho}}$ and $V_t=\sqrt{\frac{\mu}{\rho}}$, V_l and V_t are the longitudinal and transverse sound velocities in nanoparticles. Under stress free boundary conditions, Eq. (1) can be solved by introducing a scalar and vector potentials and yields two types of vibrational modes: spheroidal and torsional. These modes are described by orbital angular momentum quantum number l and harmonics n. The eigenvalue equation for the spheroidal modes is expressed as[26,30,42–44]

$$\tan\left(\frac{\omega}{V_l}a\right)\Big/\left(\frac{\omega}{V_l}a\right) = \frac{1}{1-\frac{1}{4}\left(\frac{\omega}{V_t}a\right)^2}, \quad \text{for } l=0 \qquad (2a)$$

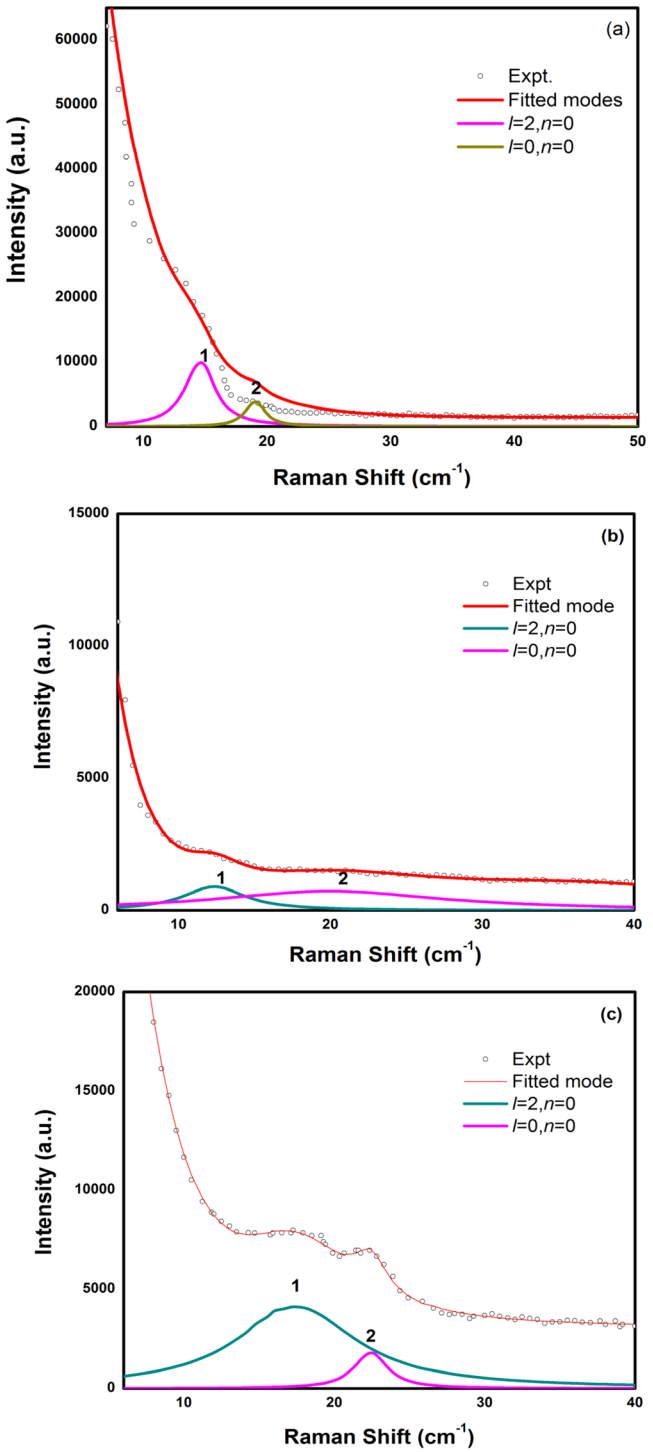

FIG. 1. Low-frequency Raman spectra of Si/Ge nanoparticles embedded in SiO_2/GeO_2 matrix: (a) Ge/SiO_2, (b) Ge/GeO_2, and (c) Si/SiO_2. Full curve: total fitted spectrum and dashed curves: individual fitted peaks. The spectra obtained with an unpolarized 532 nm wavelength laser line.

TABLE I. Eigen frequencies of spheroidal modes in (cm^{-1}) of Si/SiO_2, Ge/SiO_2, and Ge/GeO_2 of different sizes, respectively.

	Experiment		Lamb		CSM	
Sample	$l=0$ (cm^{-1})	$l=2$ (cm^{-1})	$l=0$ (cm^{-1})	$l=2$ (cm^{-1})	$l=0$ (cm^{-1})	$l=2$ (cm^{-1})
Si/SiO_2 (6 nm)	22.51	17.40	20.03	12.52	~21	–
Ge/SiO_2 (6.3 nm)	19.16	14.66	22.22	14.62	~22	–
Ge/GeO_2 (6.3 nm)	19.85	12.47	22.22	14.62	~27	–

$$2\left[\eta^2+(l-1)(l+2)\left\{\frac{\eta j_{l+1}(\eta)}{j_l(\eta)}-(l+1)\right\}\right]\frac{\xi j_{l+1}(\xi)}{j_l(\xi)} - \frac{\eta^4}{2}+(l-1)(2l+1)\eta^2 + \{\eta^2-2l(l-1)(l+2)\}\frac{\eta j_{l+1}(\eta)}{j_l(\eta)}=0, \quad \text{for } l\geq 1. \tag{2b}$$

Here η is the dimensionless eigenvalue expressed as

$$\eta_l^s=\frac{\omega_l^s R}{V_t}, \tag{3}$$

where $j_l(\eta)$ and $j_l(\xi)$ are the spherical Bessel's function of first kind and $\eta=\xi(V_t/V_l)$. The torsional modes which are orthogonal to the spheroidal modes[30,42–49] are purely transverse in nature and independent of the material property. The torsional modes are defined for $l\geq 1$. The spheroidal modes are characterized by $l\geq 0$, where $l=0$ is the symmetric breathing mode, $l=1$ is the dipolar mode, and $l=2$ is the quadrupole mode. The $l=0$ mode is purely radial and produces polarized spectra, while $l=2$ mode is quadrupolar and produces partially depolarized spectra. The spheroidal modes for even l (i.e., $l=0$ and 2) are Raman active.[19,22,33,36,41] The lowest eigenfrequencies for $n=0$ for both spheroidal and torsional modes correspond to the surface modes, while for $n\geq 1$ corresponds to inner modes.

Portalés *et al.*[43] proposed an approach known as the CSM considering nanoparticles as a core surrounded by a macroscopically large spherical matrix as a shell which leads to real valued mode frequencies[30,42–44] for calculating the absolute intensity or shape of a low frequency Raman spectrum. In this model, the motion of a nanoparticle, the mean square displacement $\langle u^2\rangle_p$ which is a measure of the internal motion of nanoparticle is obtained as a function of mode frequency. While centre position of the peak corresponds closely to the frequency obtained from Lamb's model and real part of the complex frequency from CFM.[30,42] Half widths at half maximum (HWHM) of these peaks correspond closely to the imaginary parts of the CFM frequencies.[29,37–40] Moreover, the Raman spectrum is governed by both $\langle u^2\rangle_p$ and the electron-phonon interaction matrix element. The matrix element, which appears as a multiplicative constant, determines the overall intensity while $\langle u^2(\omega)\rangle_p$ determines both the amplitude and the spectral line shape. Therefore, a preliminary step for obtaining the Raman spectrum would be to study the amplitude of the nanoparticle vibrations as a function of phonon frequency. The mean square displacement inside the nanoparticles can be written as[36,42,43]

$$\langle u^2\rangle_p=\frac{1}{\nu_p}\int_{R<R_p}|\vec{u}(\vec{R})|^2 d^3\vec{R}, \tag{4}$$

where v_p is the volume of the particle.

III. RESULTS AND DISCUSSION

Figure 1 presents the low-frequency Raman spectra from all samples measured using 532 nm wavelength. Raman scattering data are fitted to an exponential background and a Lorentzian line shape function. The present spectra are recorded in polarized configuration. The results obtained from the fitting of unpolarized spectra are presented in Table I along with the Lamb's and CSM theoretical calculations. We have used the following parameter values for the theoretical calculations: $\nu_l(Si)=9.01\times10^5$ cm/s; $\nu_t(Si)=5.37\times10^5$ cm/s; $\nu_l(Ge)=5.25\times10^5$ cm/s; $\nu_t(Ge)=3.25\times10^5$ cm/s. All spectra in Fig. 1 show two peaks indicated by the indices 1 and 2 at ~17.4, and 22.5 cm^{-1} in Fig 1(a), ~14.7 and 19.2 cm^{-1} in Fig 1(b) and ~12.5 and 19.8 cm^{-1} in Fig 1(c). The assignment of the modes is done with the help of theoretical calculations and based on the comparison of those observed frequency ratio with the calculated one. Table II presents the frequency ratio of the modes. As shown in Fig. 1 and Table I, the peaks 1 and 2 in all spectra are quadrupolar and symmetrical spheroidal mode vibrations, respectively.

Fig. 2 plots the Raman peak frequency as a function of the inverse diameter. Symbols and lines represent experimental and theoretically calculated results, respectively. This figure reveals that the calculated peak frequency which strongly depends on the particle size and increases with decreasing size is in close agreement with the experimental data. The present figure also depicts that the frequency is minimum for the fundamental quadrupolar mode. Figure also includes the peak frequency of fundamental radial and quadrupolar modes obtained by others[34–36,43] and a good agreement is observed between these and presently measured and calculated Raman peak frequencies. In addition to the evaluation of the mean diameter of particles, the low wave

TABLE II. Comparison of frequency ratio (v_o/v_2) is the frequency of the $l=2$, $n=0$; SPH mode.

Sample	Experiment (v_o/v_2)	Lamb (v_o/v_2)
Si/SiO_2 (6 nm)	1.29	1.59
Ge/SiO_2 (6.3 nm)	1.30	1.52
Ge/GeO_2 (6.3 nm)	1.59	1.52

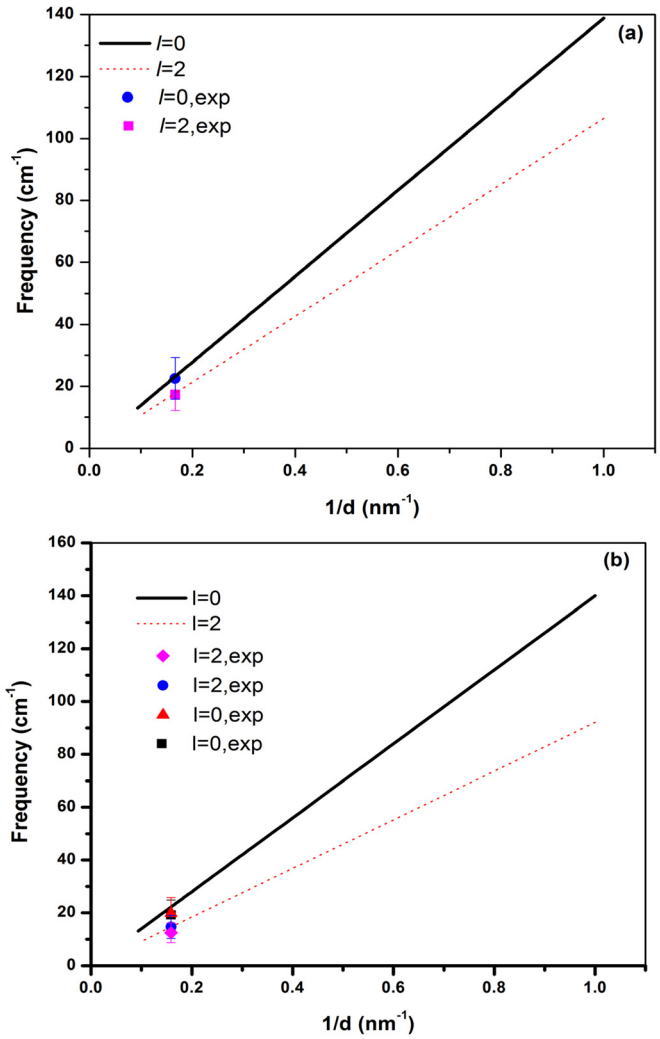

FIG. 2. Acoustic mode frequencies for SiO_2/GeO_2 embedded Si/Ge nanoparticles *Vs* 1/R; along with other experimental data: (a) Si and (b) Ge.

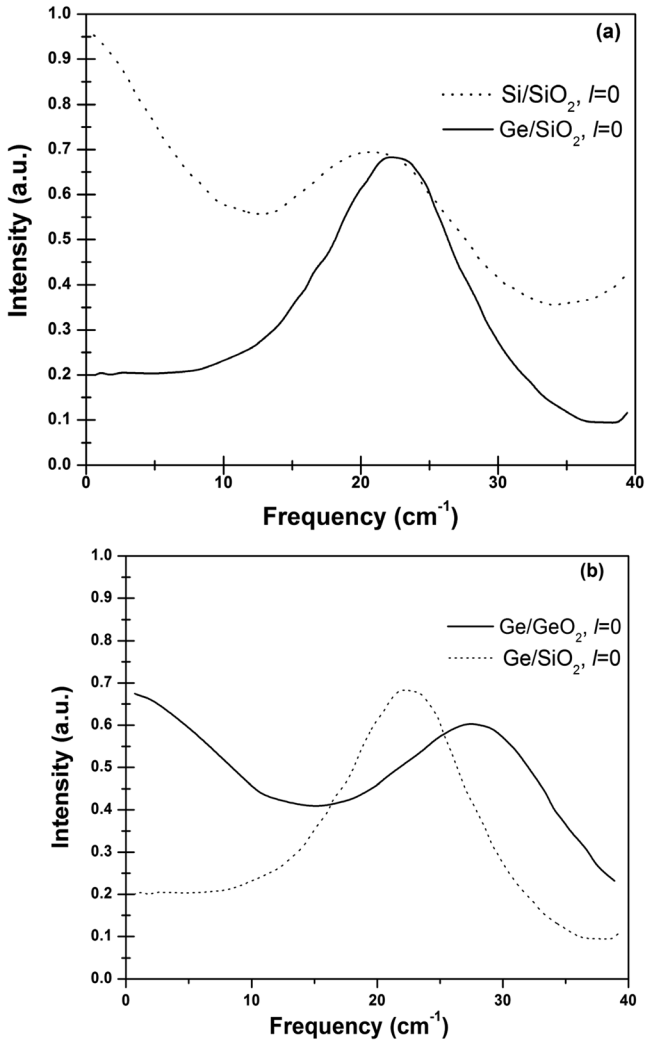

FIG. 3. Low-frequency spectra calculated using the CSM for Si/Ge nanoparticle embedded in SiO_2/GeO_2: (a) $l=0$ mode for Si/SiO_2 and Ge/SiO_2. (b) $l=0$ mode for Ge/SiO_2 and Ge/GeO_2.

number spectra can also be used to determine the size distribution of nanocrystals. In amorphous material, even without crystal nuclei, there is also an excess vibrational density of states present in a low-frequency range as compared with the Debye density, which is generally a peak in LFRS associated with phonons localization on the structure correlations of disordered materials.[35,37]

To clearly bring out the effect of matrix (hosts) on the nanoparticles, we have calculated the mean square displacement $\langle u^2 \rangle_p$ of symmetrical breathing mode ($l=0$, $n=0$) for Si and Ge nanoparticles embedded in two different hosts using core-shell model. Figure 3 shows the calculated frequency spectra by using CSM approach. In the present calculation, R_m/R_p is taken 100. Here, R_p and R_m are the radius of nanoparticle and macroscopic glass matrix. In this case, there is a continuum of states for a macroscopic glass matrix and the plots would be essentially continuous.[42] It is also seen from Fig. 3 that the broadening of peak increases in the case of elastically more similar materials.

The present paper also reports the size variation of phonon linewidth for low frequency acoustic phonon mode of Si/Ge nanoparticles embedded in SiO_2/GeO_2. The calculation of linewidth gives not only the real test of the model but also estimates damping of vibrational modes. Figure 4 presents the variation of phonon mode linewidth for $l=0$ and 2 spheroidal modes with size for the Si/Ge nanoparticle. For comparison, the present figure also includes the experimental phonon linewidth observed from the Raman scattering measurements.[18,35,36] A good agreement is observed between present and previous data. However, 1/R dependence is not clear due to the large error bars for the available range of data.

Fig. 5 presents the typical Raman spectra for the silicon and germanium nanocrystals embedded in SiO_2 and GeO_2 film. Since, the measured Raman spectra in Fig. 5 also contains the signature of amorphous SiO_2 and GeO_2 besides the strong characteristic optical phonon modes of nanocrystals Si and Ge, there are TA- like, LA- like, LO and 2TO phonon modes arising from the amorphous state of SiO_2 and GeO_2. In the case of Si nanocrystals, the peak at 520 cm^{-1} (Fig. 5(a)) which is originating from optical phonon scattering within Si nanocrystalline corresponds to the both optical phonon modes LO and TO of nc-Si at zone centre of the Brillouin zone. This is controlled by the phonon confinement effect and shows size dependent shift.[31] The other peaks at 230, 302, and 445 cm^{-1} are assigned to TA, LA, and LO like

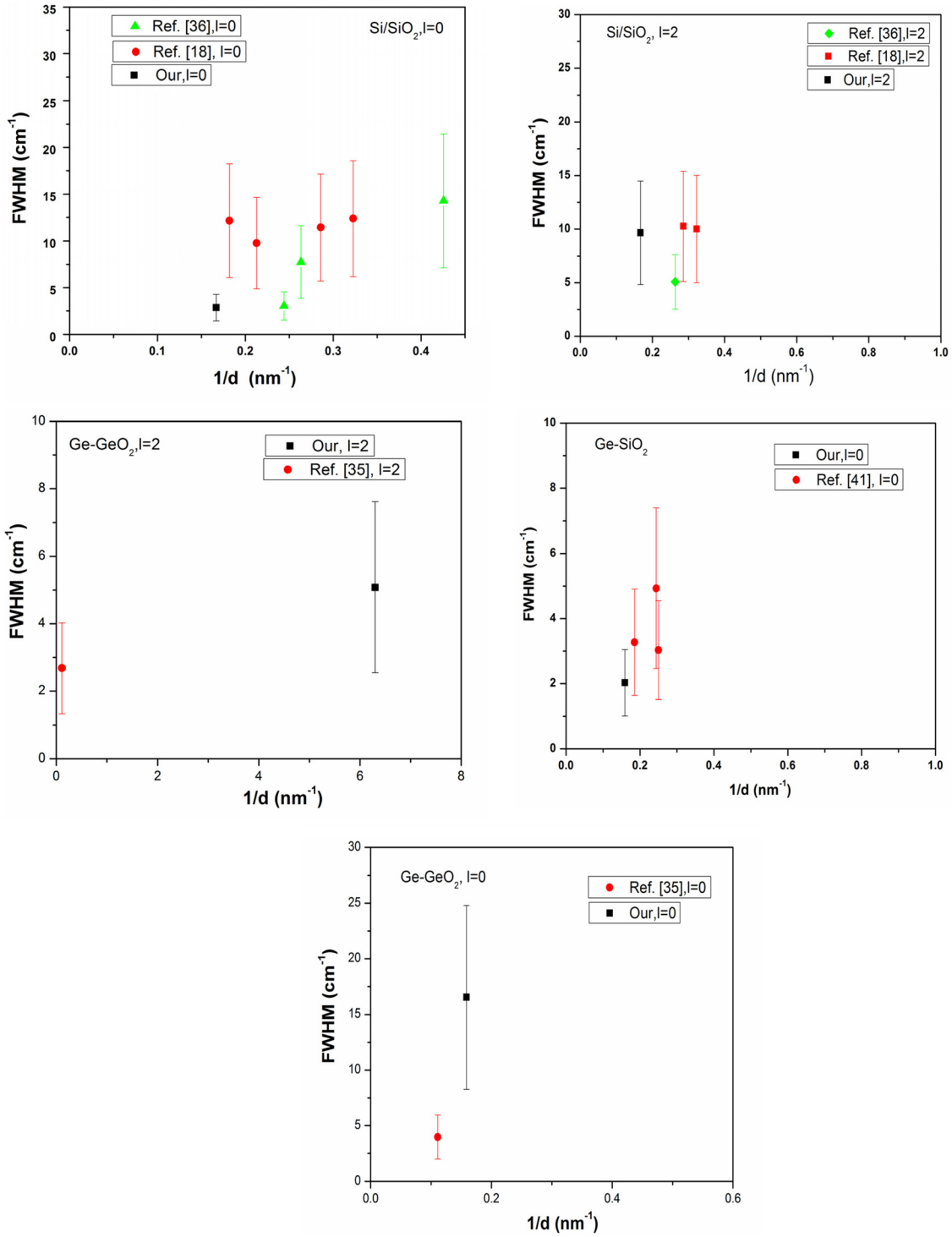

FIG. 4. Dependence of the FWHM on 1/R of the $l = 0$, $n = 0$ spheroidal phonon mode and $l = 2$, $n = 0$ Raman data along with other experimental data.

phonon modes, respectively.[50] While the peaks at 230 and 302 cm^{-1} contain contribution from nanocrystalline and amorphous phases, the peak at 445 cm^{-1} mainly comes from the LO phonons in amorphous state. The forbidden TA- and LA-like modes in spectra are due to disrupted translational symmetry and breakdown of selection rule by phonon confinement. The peaks at 618 and 980 cm^{-1} are assigned to the two phonon Raman scattering of nanocrystalline Si. The Raman scattering peaks at 618 and 980 cm^{-1} are attributed to the 2LA and 2TO like phonon modes, respectively. Ge embedded in SiO_2 presented in Fig. 5(b) shows three bands at 234, 304, and 434 cm^{-1} below the very high intense peak at 520 cm^{-1} originating from Si optical modes. The peak at 234 cm^{-1} is assigned to amorphous Ge expected due to the higher annealing temperature (above melting temperature of Ge).[51] The second band near 304 cm^{-1} is in good agreement with earlier reports[34,52] and can be associated with the characteristic optical peak of nc-Ge. The third and final peaks at 981 cm^{-1} are due to local Si-Si vibrations.[53] The presence of Si-Si bond in the Raman spectra can be attributed to the fact

that the implantation of ions produces a partial break of SiO_2 stoichiometry and resulting into a series of bonds such as Si-O, Ge-O, Si-Si, and Ge-Ge. These remarkable features alongwith the peaks at 618 and 981 cm^{-1} are attributed to the fact that the Si clusters are formed during annealing. These peaks can be assigned to 2LA and 2TO of Si like phonon modes. The similar conclusion is also drawn by Dana *et al.*[54]

The Raman spectra of Ge in GeO_2 presented in Fig. 5(c) bring out all important features of the Ge vibrations. The sharp peak centered at ~520 cm^{-1} is due to the formation of Si cluster during annealing. The contribution from Si arises due to the capping of silicon oxide on Ge/GeO_2 system. The broad peak in the spectra around 100 cm^{-1} is due to the TA-like phonon mode of nc-Ge, which is in general forbidden in one phonon Raman scattering. This forbidden first order scattering is allowed due to the disruption of translational symmetry. A broad peak at 245 and 283 cm^{-1} is due to the LA- like phonon mode and TO phonon mode of Ge, respectively. Finally, the peak at 618 cm^{-1} is due to 2TO like phonon scattering of germanium.

Our study also focuses on Raman mode lineshape analysis; in an ideal harmonic crystal, the lineshape is expected to be infinitesimally narrow, but experimental peaks of real materials exhibit an intrinsic width. On one hand, the presence of various decay channels shortens the phonon lifetime by a harmonic process involving multiple phonon recombinations conserving both energy and crystal momentum, while on the other hand, impurities and defects disturb the translation symmetry of the harmonic crystal. Therefore, they modify the Raman line width by elastic scattering processes that also contribute to the phonon-lifetime shortening scenario. The variation of the I_{2TO} /I_{1TO} ratio, which is attributed to strength of electron-phonon interaction, essentially arises due to modified matrix medium and reducing particle size. One can see the large change in the relative intensities of I_{2TO} and I_{1TO} modes for different matrix medium embedded NCs. In order to understand the e-p interaction from Raman intensities,[48,55] we have fitted the spectra using Lorentzian line shape. The absolute intensities are influenced by several external factors such as incident laser power, focusing, alignment, and detector response. Thus, the contributions to Raman intensity by these external factors get cancel out. We analyze the intensity ratio further to obtain an insight about the e-p interaction in nc-Si and nc-Ge embedded in the host matrix. From the standard equation of Raman intensity,[48,55] one can see that the intensities of the phonons are expected to differ due to the matrix element $\langle k|H_{ep}|j\rangle$ as the *e-p* interaction element $\mathbf{H}_{ep}$ is different for different phonons. Here, $|j\rangle$ and $|k\rangle$ are the intermediate electronic states. Here, phonon energy is same for all samples, the ratio of the intensities of $I_{2LO}/_{2TO}$ and $I_{1LO}/_{1TO}$ will be predominantly determined by the ratio of the corresponding matrix elements as,

$$\frac{I_{2TO}}{I_{1TO}} \approx \frac{|\langle k|H_{ep}^{2TO}|j\rangle|^2}{|\langle k|H_{ep}^{1TO}|j\rangle|^2}. \tag{5}$$

It may be pointed out for the polar LO/TO phonon both the deformation potential (DP) and the dipole-forbidden Fröhlich interaction (FI) contribute to the matrix element of e-p interaction.[48,55] On the other hand, for the non-polar I_{2TO} mode DP alone contributes to the matrix element and Eq. (5) can be written in terms of DP and FI as,

$$\frac{H_{ep}^{2TO}}{H_{ep}^{1TO}} = \frac{DP_2}{DP_1 + F_1}, \tag{6}$$

where DP_2 and DP_1 are the phonon- specific terms corresponding to the DP interaction for the I_{2TO} and I_{1TO} modes, respectively. Thus, based on the present analysis using above equations one can say that as a first approximation, the ratio of intensities presented in Table III, arising from DP and FI to the e-p interaction. However, the electron-phonon coupling can be estimated by measuring the normalized Raman intensities of the 2TO phonon with respect to that of the 1TO phonon.

Table III reveals two interesting points about the ratio of Raman intensity: (i) it is higher for Ge than Si and (ii) it is higher in the case of dissimilar medium.[55–58] The higher intensities correspond to high *e-p* interaction in Ge/SiO_2 and may be attributed to two primarily reasons: (i) suppression of Ge desorption as compared with Si, resulting higher density of Ge nanocrystals[25] (ii) the acoustic impedance resulting from the spatial confinement of acoustic phonons. This suggests that the e-p coupling strength is more if one considers nanocrystals embedded with elastically dissimilar material. This e-p interaction (coupling strength) might also be responsible for the increase in FWHM of $l = 0$ spheriodal modes in Fig. 3. In the case of embedded NCs, the phonon depletion with corresponding scattering rate suppression can be

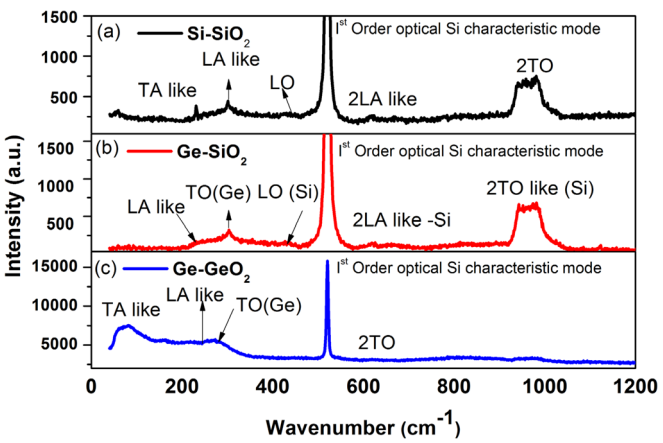

FIG. 5. Optical Raman spectra for Si/SiO_2, Ge/SiO_2 and Ge/GeO_2.

TABLE III. Comparison ratio of intensity ratio of Si/SiO_2, Ge/SiO_2, and Ge/GeO_2.

Intensity ratio	Si/SiO_2	Ge/SiO_2	Ge/GeO_2
I_{2TO}/I_{1TO}	0.039	1.953	0.571

achieved in acoustically harder material, while the phonon accumulation occurs in the acoustically softer material.[49]

IV. CONCLUSION

Low frequency acoustic phonon modes have been investigated for the Si and Ge nanoparticles embedded in two different hosts (matrix) such as SiO_2 and GeO_2 glass using the low frequency Raman scattering and two different models, namely, the classical Lamb's model and the core shell model. The low frequency Raman spectra for all three samples consists two peaks which have been assigned to breathing and quadrupolar modes using calculated spheroidal mode frequencies and ratio of two consecutive modes. Size dependent line width and frequency of spheroidal modes have been also analyzed. There is a good agreement between the present and previous studies. Line width increases in the case of elastically similar material. This is due to the fact that when the acoustic impedences ($Z = \rho V_L$; ρ is density and V_L is longitudinal sound velocity for nanoparticles and medium match reflection of sound waves is negligible. As the acoustic impedance mismatch increases, acoustic wave reflection increases leading to more pronounced nanoparticle modes. Besides the low frequency Raman spectra, the peaks in optical phonon Raman scattering are also assigned and used to calculate the electron-phonon interaction ratio of Raman intensities. The peaks assigned in the Raman spectra are quite similar to the previous studies. Our results finally reveal that the nanocrystals embedded in elastically dissimilar materials have higher electron-phonon coupling strength. This can be useful for the development of devices where electron-phonon interaction plays an important role.

ACKNOWLEDGMENTS

The financial assistance from BRNS, Department of Atomic Energy and DST-RFBR is highly appreciated. VM and PKJ acknowledge CSIR, New Delhi for the award of senior Research Fellowship and UGC, New Delhi for UGC Research Award, respectively.

[1]G. Ledoux, J. Gong, F. Huisken, O. Guillois, and C. Reynaud, Appl. Phys. Lett. **80**, 4834 (2002).
[2]D. J. Lockwood, Z. H. Lu, and J. M. Baribeau, Phys. Rev. Lett. **76**, 539 (1996).
[3]G. Ledoux, O. Guillois, C. Reynaud, F. Huisken, B. Kohn, and V. Paillard, Mater. Sci. Eng., B **69**, 350 (2000).
[4]V. Paillard, P. Puech, M. A. Iaguna, R. Carles, B. Kohn, and F. Huisken, J. Appl. Phys. **86**, 1921 (1999).
[5]T. Usuki, T. Futatsugi, and N. Yokoyama, Microelectron. Eng. **47**, 281 (1999).
[6]H. Takagi, H. Ogawa, Y. Yamazaki, A. Ishizaki, and T. Nakagiri, Appl. Phys. Lett. **56**, 2379 (1990).
[7]Y. Maeda, Phys. Rev. B **51**, 1658 (1995).
[8]S. Takeoka, M. Fujii, S. Hayashi, and K. Yamamoto, Phys. Rev. B **58**, 7921 (1998).
[9]G. Franzo, E. C. Moreira, D. Pacifici, F. Priolo, F. Iacona, and C. Spinella, Nucl. Instrum. Methods Phys. Res. B **175**, 140 (2001).
[10]A. Markwitz, L. Rebohle, H. Hofmeister, and W. Skorupa, Nucl. Instrum. Methods Phys. Res. B **147**, 361 (1999).
[11]T. Bostedt, T. van Burren, M. Willey, N. Franco, L. J. Terminello, C. Heske, and T. Moller, Appl. Phys. Lett. **84**, 4056 (2004).
[12]J. R. Heath, J. J. Shiang, and A. P. Alivisatos, J. Chem. Phys. **101**, 1607 (1994).
[13]K. S. Min, K. V. Shcheglov, C. M. Yang, H. A. Atwater, M. L. Brongersma, and A. Polman, Appl. Phys. Lett. **68**, 2511 (1996).
[14]X. L. Wu, Y. F. Mei, G. G. Siu, K. L. Wong, K. Moulding, M. J. Stokes, C. L. Fu, and X. M. Bao, Phys. Rev. Lett. **86**, 3000 (2001).
[15]L. Saviot, N. Combe, and A. Mlayah, Phys. Rev. B **85**, 075405 (2012).
[16]A. Courty, P. Mermet, A. Albouy, E. Duval, and M. P. Pileni, Nature Mater. **4**, 395 (2005).
[17]E. Duval, A. Boukenter, and B. Champagnon, Phys. Rev. Lett. **56**, 2052 (1986).
[18]M. Fujii, T. Nagareda, S. Hayashi, and K. Yamamoto, Phys. Rev. B **44**, 6243 (1991).
[19]S. Tanaka, Onari, and T. Arai, Phys. Rev. B **47**, 1237 (1993).
[20]L. Saviot and D. B. Murray, Phys. Rev. Lett. **93**, 055506 (2004).
[21]X. L. Wu, S. J. Xiong, Y. M. Yang, J. F. Gong, H. T. Chen, J. Zhu, J. C. Shen, and P. K. Chu, Phys. Rev. B **78**, 165319 (2008).
[22]H. K. Yadav, V. Gupta, K. Sreenivas, S. P. Singh, B. Sundarakannan, and R. S. Katiyar, Phys. Rev. Lett. **97**, 085502 (2006).
[23]K. T. Tsen, E. C. Dykeman, O. F. Sankey, S. W. D. Tsen, N. T. Lin, and J. G. Kiang, Nanotechnology **17**, 5474 (2006).
[24]T. M. Liu, H. P. Chen, L. T. Wang, J. R. Wang, T. N. Luo, Y. J. Chen, S. I. Liu, and C. K. Sun, Appl. Phys. Lett. **94**, 043902 (2009).
[25]N. P. Stepina, A. V. Dvurechenskii, V. A. Armbrister, V. G. Kesler, P. L. Novikov, A. K. Gutakovskii, V. V. Kirienko, Zh. V. Smagina, and R. Groetzschel, Appl. Phys. Lett. **90**, 133120 (2007).
[26]H. Lamb, Proc. London Math. Soc. **13**, 189 (1882).
[27]A. Dieguez, J. Romano-Rodriguez, R. Morante, N. Barsan, U. Weimar, and W. Gopel, Appl. Phys. Lett. **71**, 1957 (1997).
[28]E. Duval, H. Portales, L. Saviot, M. Fujii, K. Sumitomo, and S. Hayashi, Phys. Rev. B **63**, 075405 (2001).
[29]P. K. Jha, Indian J. Pure Appl. Phys. **44**, 87 (2006).
[30]S. K. Gupta, S. Sahoo, P. K. Jha, A. K. Arora, and Y. M. Azhniuk J. App. Phys. **106**, 024307 (2009); S. K. Gupta, P. K. Jha, and A. K. Arora, J. Appl. Phys. **103**, 124307 (2008).
[31]S. K. Gupta and P. K. Jha, Solid State Commun. **149**, 1989 (2009).
[32]F. Q. Liu, L. S. Liao, G. H. Wang, G. X. Cheng, and X. M. Bao, Phys. Rev. Lett. **76**, 604 (1996).
[33]E. Duval, Phys. Rev. B **46**, 5795 (1992).
[34]X. L. Wu, G. G. Siu, X. Y. Yuan, N. S. Li, Y. Gu, X. M. Bao, S. S. Jiang, and D. Feng, Appl. Phys. Lett. **73**, 1568 (1998).
[35]N. N. Ovsyuk and V. N. Novikov, Phys. Rev. B **53**, 3113 (1996).
[36]M. Ivanda, A. Hohl, M. Montagna, G. Mariotto, M. Ferrari, Z. Crnjak Orel, A. TurkovicôĈ, and K. Furic, J. Raman Spectrosc. **37**, 161–165 (2006).
[37]N. N. Ovsyuk, V. Mankad, S. K. Gupta, P. K. Jha, and G. A. Kachurin, Bull. Russ. Acad. Sci. Phys. **75**, 601–604 (2011).
[38]W. Cheng and S. F. Ren, Phys. Rev. B **65**, 205305 (2002); W. Cheng, S. F. Ren, and P. Y. Yu, *ibid.* **68**, 193309 (2003).
[39]G. A. Kachurin, S. G. Yanovskaya, K. S. Zhuravlev, and M. O. Ruault, Fiz. Tekh. Poluprovodn. (St. Petersburg) **35**, 1235 (2001); Semiconductors **35**, 1182 (2001).
[40]G. A. Kachurin, V. A. Volodin, D. I. Tetel'baum, D. V. Marin, A. F.Leĭer, A. K.Gutakovskiĭ, A. G. Cherkov, and A. N. Mikhaĭlov Semiconductors **39**, 552 (2005).
[41]P. K. Giri, R. Kesavamoorthy, B. K. Panigrahi, and K. G. M. Nair, Solid State Commun. **136**, 36 (2005).
[42]V. A. Dubrovskiy and V. S. Morochnik, Izv., Acad. Sci., USSR, Phys. Solid Earth **17**, 494 (1981).
[43]H. Portalés, L. Saviot, E. Duval, M. Gaudry, E. Cottanum, M. Pellarin, J. Lerme, and M. Broyer, Phys. Rev. B **65**, 165422 (2002).
[44]Y. Li, H. S. Lim, S. C. Ng, and M. H. Kuok, Chem. Phys. Lett. **440**, 321 (2007).
[45]M. Montagna and R. Dusi, Phys. Rev. B **52**, 10080 (1995).
[46]M. Montagna, Phys. Rev. B **77**, 167401 (2008).
[47]M. Montagna, Phys. Rev. B **77**, 045418 (2008).
[48]A. Pinczuk, E. Burstein, "Light scattering in solids," in *Topics in Applied Physics*, edited by M. Cordona, Vol. 8 (Springer, Berlin, 1975), p. 38.
[49]A. A. Balandin, E. P. Pokatilov, and D. L. Nika, J. Nanoelectron. Optoelectron. **2**, 140 (2007).
[50]M. A. Zhixun, L. Xianbo, K. Guanglin, and C. Junhao, Sci. China **43**, 414 (2000).
[51]J. G. Zhu, C. W. White, J. D. Budai, S. P. Withrow, and Y. Chen, J. Appl. Phys. **78**, 4386 (1995).

[52]X. L. Wu, T. Gao, X. M. Bao, F. Yan, S. S. Jiang, and D. Feng, J. Appl. Phys. **82**, 2704 (1997).
[53]A. V. Kolobov, J. Appl. Phys. **87**, 2926 (2000).
[54]A. Dana, S. Agan, S. Tokay, A. Aydinli, and T. G. Finstad, Phys. Status Solidi C **4**, 288 (2007).
[55]S. Sahoo, V. Sivasubramanian, S. Dhara, and A. K. Arora, Solid State Commun. **147**, 271 (2008).
[56]See http://www.ioffe.ru/SVA/NSM/Semicond/. This website is intended to systematize parameters of semiconductor compounds and heterostructures based on them. Such a WWW-archive has a number of advantages: in particular, it enables physicists, both theoreticians and experimentalists, to rapidly retrieve the semiconducting material parameters they are interested in. In addition, physical parameters – optical, electrical, mechanical, etc. – will be presented in the framework of the electronic archive for both the known and new semiconducting compounds. The voluminous reference book "Handbook Series on Semiconductor Parameters" vol. 1,2 edited by M. Levinstein, S. Rumyantsev and M. Shur, World Scientific, London, 1996, 1999, served as the starting point in creating the database.
[57]Y. D. Glinka and M. Jaroniec, J. Phys. Chem. B **101**, 8832 (1997).
[58]J. F. Scott, Phys. Rev. B **1**, 3488 (1970).